Sustainable Materials and Technologies 25 (2020) e00198

Contents lists available at ScienceDirect

Sustainable Materials and Technologies

journal homepage: www.elsevier.com/locate/susmat

Fast and cost-effective room temperature synthesis of high quality graphene oxide with excellent structural intactness

Jiadong Qin [a], Yubai Zhang [a], Munkhbayar Batmunkh [a], Ge Shi [a], Mohammad Al-Mamun [a], Porun Liu [a], Wei Li [b], Dong-Chen Qi [b], Huijun Zhao [a,*], Yu Lin Zhong [a,*]

[a] Centre for Clean Environment and Energy, School of Environment and Science, Griffith University, Gold Coast, Queensland 4222, Australia
[b] School of Chemistry and Physics, Queensland University of Technology, Brisbane, Queensland 4001, Australia

ARTICLE INFO

Article history:
Received 5 June 2020
Received in revised form 18 June 2020
Accepted 6 July 2020

ABSTRACT

Graphene oxide (GO) is well known as a key material to the commercialization of graphene-based applications due to its excellent processability and abundant starting materials. However, producing high quality GO with excellent structural intactness still remains a challenge despite the significant research effort over the past decade. Herein, we demonstrate an effective approach to achieving well-oxidized GO within only 5 h of oxidation time at 5 °C or 25 °C from expanded graphite as a starting material. Our finding reveals that the well-oxidized GO synthesized at 25 °C can regain more graphitic sp^2 networks and thus becomes as conductive as the GO prepared at 5 °C by means of thermal annealing or green chemical reduction. We also found that green chemical reduction using vitamin C (VC) is more efficient in restoring the electrical conductivity and reducing the defects in the GO produced at room temperature. The protocol reported in this paper offers a promising, sustainable way to fabricate high quality GO with minimal energy input, while being cost-effective.

1. Introduction

Since the discovery in 2004, graphene, a monolayer of carbon atoms arranged in hexagonal rings, has been sitting in the spotlight owing to its fascinating properties [1,2]. As the most important graphene derivatives, graphene oxide (GO) and its reduced form, reduced graphene (rGO), have been the subject of intense exploration and achieved great success in a diverse range of applications, ranging from energy-storage and -conversion devices [3,4] to ionic and molecular sieving membranes [5,6] to biomedical applications [7–10]. The ultimate goal of developing these applications is to promote the broad commercialization of graphene-based products with high performance and cost-effectiveness [11]. In order to realize this goal, the scalable and cost-effective fabrication of GO materials is of significant importance [12]. Currently, the exfoliation of chemically oxidized graphite into single layers using the $KMnO_4$-based Hummers method [13], namely the graphite oxide route, is the most extensively used method to produce GO in bulk [12]. Typically, it involves the edge-to-core diffusion of oxidizing agents in the narrow graphite interlayer galleries, which determines the reaction rate of forming GO [14]. To facilitate the conversion of graphite into GO, one common strategy is to pre-intercalate graphite with foreign species which enables to expand the interlayer spacings [15–18]. The spacing expansion is more dramatic when gasifying the thermo-decomposable intercalants, namely forming the expanded graphite [19,20]. In addition, applying external heating (≥ 35 °C) can thermodynamically favor the diffusion process [21,22]. Owing to the inexpensive sources, good dispersibility, rich oxygen functional groups and high product yield, graphite oxide route has been successfully scaled up from lab-scale researches to industrial mass production [12,23].

Despite its preliminary commercialization, the graphite oxide route with harsh oxidation conditions, such as the use of strong acids, oxidants and heating, usually introduces uncontrollable functionalities and enormous permanent defects into final products. This will result in poor electronic properties of rGO, including electrical conductivity and charge-carrier mobility, which are undesirable for electro-conductive applications [24]. To preserve the sp^2 honeycomb structure in graphene basal plane, using low reaction temperature (<0 °C) in the graphite oxide route can effectively minimize the loss of carbon atoms in the GO. The resulting highly intact rGO exhibited excellent electronic properties that are comparable to the pristine graphene [25–27]. However, the low temperature modified methods are of higher cost due to the necessity for low temperature control, poor GO yield (<50%) and significantly more time-consuming process (>1 day per batch).

To obtain high quality GO without compromising cost-effectiveness, our group recently reported a simple but effective method to synthesize GO with rich thermally labile oxygen functional groups from

* Corresponding authors.
E-mail addresses: h.zhao@griffith.edu.au (H. Zhao), y.zhong@griffith.edu.au (Y.L. Zhong).

https://doi.org/10.1016/j.susmat.2020.e00198
2214-9937/

pre-intercalated graphite at room temperature (25 °C) [28]. In comparison to the conventional graphite oxide routes (reaction temperature ≥ 35 °C), the advantages of our approach are that the resultant GO is not only less defective but also restores more electrical conductivity after simple thermal annealing at only 150 °C in ambient air. This makes the room temperature GO (RT-GO) more conducive and cost-effective to electroconductive applications relative to the traditional GO. For example, RT-GO can be blended well into composite slurry and converted to conductive binders in lithium ion batteries after mild annealing at 150 °C [28]. The benefits of the facile deoxygenation and high structural integrity of RT-GO have also been demonstrated by Li and co-workers [29]. Furthermore, it is worth noting that the RT-GO prepared by Li's group, which was oxidized for 3 h, exhibited comparable defect density and electrical conductivity to the GO oxidized at 5 °C for 12 h (low T-GO) after chemical reduction.

The diffusion of oxidants in natural graphite or pre-intercalated graphite proceeds in a noticeably slower manner at room temperature and below, thus requiring much longer reaction time [14,28,30]. To address this issue, the use of expanded graphite with larger inter-galleries spacing as the starting material is likely to facilitate the propagation of oxidation under mild conditions [19,20,31–34]. Herein, we demonstrated that the conversion of expanded graphite into monolayered GO can be accomplished within only 5 h at both 5 °C (low temperature) and 25 °C (room temperature). Further, this enabled the direct comparisons between RT-GO and low T-GO under the same reaction conditions except for temperature. We further found that in spite of its higher oxidation degree and lower electrical conductivity, RT-GO could regain considerably more electrical conductivity as compared to the low T-GO after a simple thermal treatment at 150 °C or mild chemical reduction by vitamin C (VC). In addition, VC was found to be more efficient for the restoration of conductivity than the mild thermal annealing process. Extensive characterizations revealed that more conjugated sp^2 carbon networks and less defective structure recovered from VC reduction led to the greater increase in the conductivity of the RT-GO with respect to that of the low-T GO. On account of the mild but efficient oxidation process coupled with eco-friendly reduction methods, it is expected that the RT-GO derived from expanded graphite will offer significant advantages towards the bulk-scale, sustainable production of graphene materials at low cost for electroconductive applications.

2. Experimental

2.1. Materials

Expanded graphite powder (≥ 99% carbon, 6 μm) was purchased from Qingdao FRT Graphite Co. Ltd. $KMnO_4$ (99.0%), concentrated H_2SO_4 (98%), aqueous H_2O_2 solution (30% *w*/w), *N,N*-dimethylformamide (DMF), ethanol (undenatured, 100%) and hydrochloric acid (32 wt%) were all purchased from Chem-Supply. Vitamin C (L-ascorbic acid, $C_6H_8O_6$) was purchased from Ajax Chemicals. Deionized (DI) water was used in all experimental procedures, including the synthesis reaction and purification.

2.2. Synthesis of RT-GO and low-T GO

GO samples were prepared from expanded graphite according to our recent protocol based on the modified Hummers method [28], while the ice bath was replaced with a chiller-controlled 5 °C water bath. For the preparation of RT-GO, the reaction system was placed in the 5 °C water bath in the first hour. Then, the temperature was increased to 25 °C at which point the reaction system was stirred for a specified period (2 h, 4 h and 8 h) before exposed to water-induced hydrolysis. Depending on the period of oxidation, the resulting GO were termed as GO-25C3h, GO-25C5h and GO-25C9h, respectively. On the other hand, for the low T-GO, the entire reaction process was carried out in the 5 °C water bath for 5 h, followed by water-induced hydrolysis. The product was denoted as GO-5C5h. After the purification, GO was homogeneously dispersed in 200 mL DI water by magnetic stirring and then 5 mL GO dispersion was collected to deposit onto a nylon membrane (average pore size: 0.22 μm) by vacuum filtration, followed by drying in an oven at 60 °C overnight. The polymer membrane was then gently peeled off. The weight of the freestanding GO films can be used to measure the concentration of GO dispersion (C_{GO}, mg/mL). Moreover, the yield of GO can be measured based on the total volume of the purified GO dispersion (200 mL) and the mass of the starting graphite (1 g). All samples were stored in a refrigerator at 4 °C.

2.3. Reduction of the free-standing GO films

Mild thermal annealing and green chemical reduction were used to reduce the free-standing GO films. The good dispersibility of GO in water allows it to form a smooth membrane with even thickness, which is key to the reliable measurement of sheet resistance. The thermal annealing of GO films was carried out in the 150 °C oven for 5 h in ambient air. For the chemical reduction, GO films were dipped in a VC aqueous solution (10 mg/mL) for 24 h, followed by washing with excess DI water to remove the residual VC solution. Then the VC reduced GO films were dried in the 60 °C oven overnight.

2.4. Characterizations

X-ray diffraction (XRD) spectra were measured using a Bruker D8 advance diffractometer with Cu Kα radiation (λ = 1.5418 Å). The elemental analysis of GO and rGO samples were carried out using X-ray photoelectron spectroscopy (XPS) with the Kratos Axis Ultra using a monochromatized Al K_α x-ray source. For XPS spectra, the binding energy scales were all calibrated by aligning the dominant graphitic carbon (C=C/C-C) peak at the position of 284.6 eV. Raman spectroscopy was conducted on the free-standing GO and rGO films employing a Renishaw inVia Raman microscope with a 532 nm laser source. UV–vis spectroscopy of the GO aqueous dispersion was performed on an Agilent Cary 5000 spectrophotometer. Scanning electron microscopy (SEM) was conducted on a Joel JSM-7500FA microscopy with an accelerating voltage of 15.0 kV. Atomic force microscopy (AFM) images were collected on a Bruker Dimension Icon AFM using a peak force tapping mode. The lateral dimensions of graphite sources were observed through an optical microscope (Olympus LEXT OLS5000). The samples for the SEM and AFM were prepared by spin-coating diluted GO dispersion (~0.1 mg/mL, mixed solvent: 50 vol% ethanol +50 vol% DI water, sonicated for 30 min) onto a silicon wafer. The statistical analysis of the number of layers was carried out based on the line profiles of more than 120 pieces of GO sheets from AFM images. To track the weight loss during the heating, thermogravimetric analysis (TGA) was performed using a Netzsch STA 449F3 analyzer under pure argon (Ar) atmosphere. For the TGA test, GO samples were gradually heated from 50 to 1000 °C at the rate of 5 K/min. The electrical conductivity of the GO and rGO films were measured using a Jandel RM3000 four-point probe system with a linear arrayed head (probe spacing of 1 mm). The film thicknesses were measured to be around 30 μm using a micrometer (resolution 0.001 mm). The conductivity measurement was based on the conversion of sheet resistance (Ω per square) of multiple points on a single film into the electrical conductivity (S/m).

3. Results and discussion

3.1. Chemical properties of as-prepared RT-GO and low T-GO

In this work, we prepared GO samples using two different oxidation temperatures, namely 5 °C and 25 °C, from expanded graphite (see experimental detail). XRD was used to investigate the conversion of expanded graphite to graphite oxide, as shown in Fig. 1a. As compared to the original expanded graphite, all GO samples lost the strong

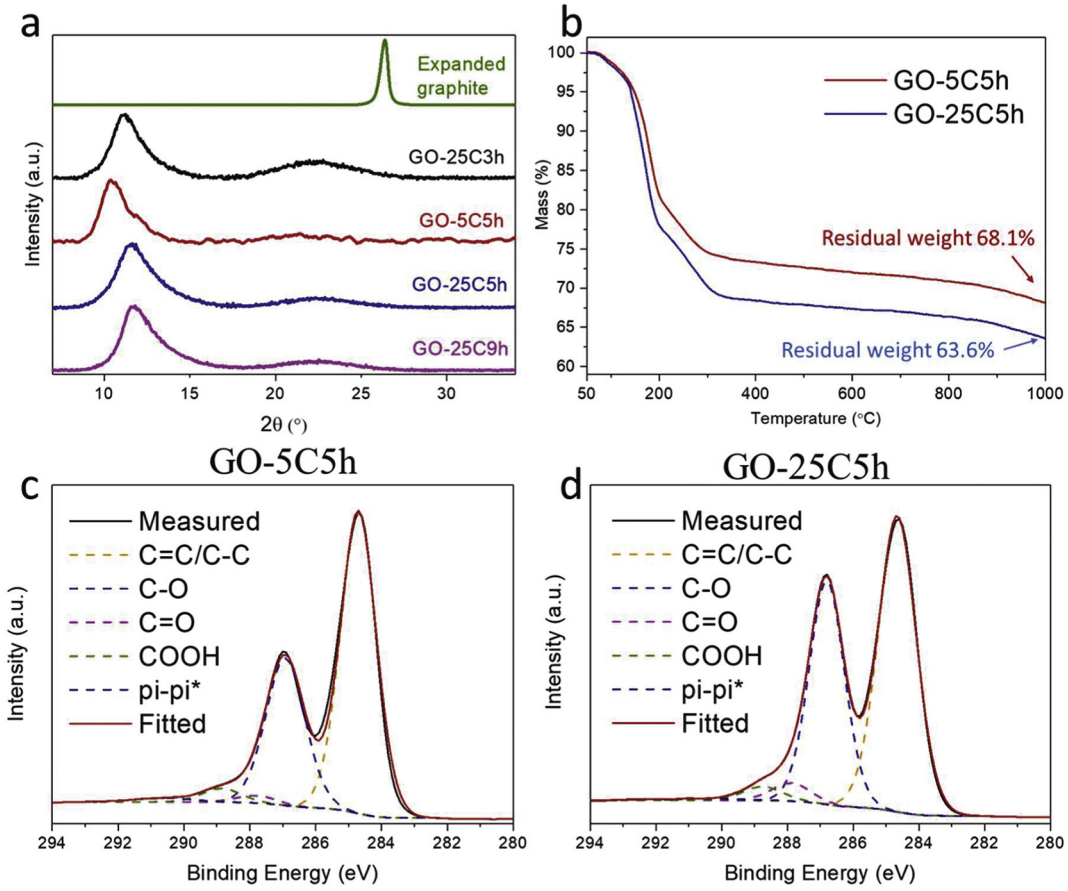

Fig. 1. Chemical characterizations of various GO samples. (a) XRD patterns for the starting expanded graphite and GO. (b-c) High resolution XPS C 1 s spectra with deconvolution to indicate the contributions from different carbons. (d) TGA curves for GO-5C5h and GO-25C5h measured in pure argon at a heating rate of 5 K/min.

graphitic peak at 26.4°, which can be associated with the interlayer spacing between unoxidized graphene sheets (3.46 Å). Instead, the main characteristic peak at around 11° appeared for all samples, indicative of an expanded interlayer spacing after oxidation (~ 8.04 Å). In addition, GO samples showed a weak broad peak centered at around 22° (see Fig. S1), and it is attributed to the less oxidized parts in GO [35–37]. For the GO oxidized at 25 °C, the intensity of this broad peak is highest in GO-25C3h and decreases to the same level in both GO-25C5h and GO-25C9h. This implies the content of the less oxidized GO has reached the minimum when the oxidation time is 5 h. In the case of the mild oxidation at 5 °C, the GO-5C5h exhibited a similar proportion of less oxidized parts to the GO-25C5h and GO-25C9h. Therefore, it can be concluded that the conversion to GO was completed for the GO-5C5h, GO-25C5h and GO-25C9h. The freeze-dried powders of these three GO samples can be readily re-dispersed in a 50 vol% ethanol/water solvent, forming black dispersions of concentration of 0.1 mg/mL (Fig. S2). We also compared the XRD patterns of our expanded graphite-derived GO (GO-25C9h) with the GO produced from pre-intercalated graphite, as reported in our previous work, using the same experimental conditions (Fig. S3) [28]. It is apparent that, although the pre-intercalated graphite was much larger in flake size (Fig. S4), the resultant GO from it had a smaller proportion of less-oxidized regions relative to that from the expanded graphite. This is possibly due to the lower acid wettability of porous expanded graphite with some trapped air, which leads to limited accessible diffusion paths for oxidizing agents [14].

More in-depth chemical information of our GO-5C5h, GO-25C5h and GO-25C9h can be revealed from the TGA and XPS characterizations (Fig. 1b-d and Figs. S6-S7). TGA results (Fig. 1b) confirmed that GO-5C5h was less oxygen functionalized than GO-25C5h since the former retained higher residual mass at higher temperatures (>150 °C) in pure argon atmosphere. In addition, the sharpest weight loss occurred between 136 °C and 200 °C for both GO-5C5h and GO-25C5h, suggesting similar thermally labile oxygen functional groups were presented in both samples. From the XPS survey spectra (Fig. S6), GO-5C5h showed a C/O ratio of 4.05, which was higher than that of the GO-25C5h (3.40) and GO-25C9h (3.17). The high C/O ratio indicates the limited oxygen functionalization at 5 °C, thus contributing to the lowest GO yield for GO-5C5h as shown in Table S1. The XPS C 1 s spectra (Fig. 1c-d and Fig. S7) can be deconvoluted into five components: C=C/C-C (284.6 eV), C—O (286.8 eV), C═O (287.8 eV), COOH (288.8 eV) and π-π*satellite (290.6 eV) [38–40]. According to the deconvolution results (Table S2), GO-5C5h evidently retained higher fraction of sp^2 conjugated carbon (61.13 at.%), as compared to the GO-25C5h (54.62 at.%) and GO-25C9h (52.65 at.%). Meanwhile, the π-π* satellite tail towards higher binding energy was more pronounced in GO-5C5h, correlated to more π conjugated network, in comparison to the other two GO samples produced at room temperature [41]. The UV–vis spectra (Fig. S8) of diluted GO dispersion shows obvious redshift occurred in the absorption peak (~ 250 nm) of GO-5C5h relative to GO-25C5h and GO-25C9h. This is indicative of larger conjugated graphitic domains in the GO-5C5h [18], consistent with the XPS results.

Apart from different functionalities, the differences between the structures of GO-5C5h and GO-25C5h can be revealed from their Raman spectra (Fig. S9), which involve the defect-activated D band (1340 cm^{-1}) and the sp^2 carbon-related G band (1590 cm^{-1}) [42]. It is predicted that GO-25C5h was more defective than GO-5C5h since more defects would be introduced to GO along with the depletion of carbon atoms from graphene backbone during higher temperature oxidation [25,26]. This is evidenced by the wider D band for GO-25C5h,

which is associated with more disordered and defective structures [43,44]. In addition, the intensity ratio of D band to G band (I_D/I_G), which can be calculated from a two-component fitting, is lower in GO-25C5h (0.99) compared to GO-5C5h (1.18). According to Ferrari et al. [43,45–48], the variation of I_D/I_G would experience two distinct stages during the gradual conversion of graphite into GO. In the first stage, the I_D/I_G increases with defect density at a low defect concentration. Upon reaching a critical defect concentration, however, the I_D/I_G starts to decrease in the second stage. Therefore, it is reasonable to conclude that both GO-5C5h and GO-25C5h were in stage 2.

3.2. Morphological characterizations of low T-GO and RT-GO

In order to investigate the morphology of our GO sheets, the as-prepared diluted dispersions of GO-5C5h and GO-25C5h (~ 0.1 mg/mL) were spin coated onto a Si/SiO_2 wafer for SEM and AFM characterizations. First, from the particle size analysis based on the SEM images (Fig. 2a-b), both samples shared the similar distributions of lateral dimensions, particularly 1.18 ± 0.97 μm for GO-5C5h and 1.37 ± 1.13 μm for GO-25C5h (average ± standard deviation). Second, the thickness of individual sheets can be revealed from AFM imaging. As is evident in Fig. 2c-f and Fig. S10, nearly 90% of GO-5C5h and GO-25C5h flakes can be exfoliated into a single layer with a thickness of 1.2–1.6 nm [49]. The minor presence of few- or multi-layered GO (≥ 3 layers) is possibly caused by the less oxidized parts or restacked sheets during the rapid drying.

3.3. Electrical conductivity of low T-GO and RT-GO before and after reduction

To restore the electrical conductivity of GO, reduction methods with low cost, environmental friendliness and broad applicability are preferred [28,50–55]. Here we reduced our GO samples, in the form of freestanding membranes, using a mild thermal treatment in a 150 °C oven for 5 h in ambient air [28], or a green chemical method based on VC which is commonly recognized as a safe but effective reductant [56–58]. For the chemical reduction, GO samples were soaked in the VC aqueous solution (10 mg/mL) for 24 h, followed by rinsing in DI water and drying in a 60 °C oven.

The changes in the electrical conductivity and the corresponding film thicknesses of GO-5C5h and GO-25C5h are displayed in Fig. 3 and Table S3. In contrast to the slight change in the film thicknesses, a considerable enhancement in the conductivity of both GO films was observed. In the as-synthesized state, the GO-5C5h (3207 S/m) was five times more conductive than the GO-25C5h (576 S/m), attributed to the higher content of conducting sp^2 conjugated carbon (as demonstrated in the XPS results). As for the deoxygenated state, it is observed that the VC reduction (> 40,000 S/m) can recover more conductivity than the thermal conversion (~ 20,000 S/m). Moreover, a more striking enhancement in the conductivity was observed for the GO-25C5h after both thermal conversion and chemical reduction, resulting in rGO-25C5h as conductive as rGO-5C5h. This indicates that the structural intactness of GO-25C5h is similar to CH-5C5h and could restore more sp^2 carbon as compared to the GO-5C5h during the reduction. We also compared the electrical conductivity of our reduced GO-25C5h with previously reported rGO (Table S4). It clearly demonstrates that our reduced GO-25C5h prepared based on room temperature oxidation shows the advantages of not only energy-saving and environmentally-friendly processing, but can also exhibit comparable or even higher conductivity than those in the literature.

3.4. Chemical properties of reduced low T-GO and RT-GO

The dramatic change in the conductivity arises from the transformed chemical properties of GO, namely the oxygen functionalities and the

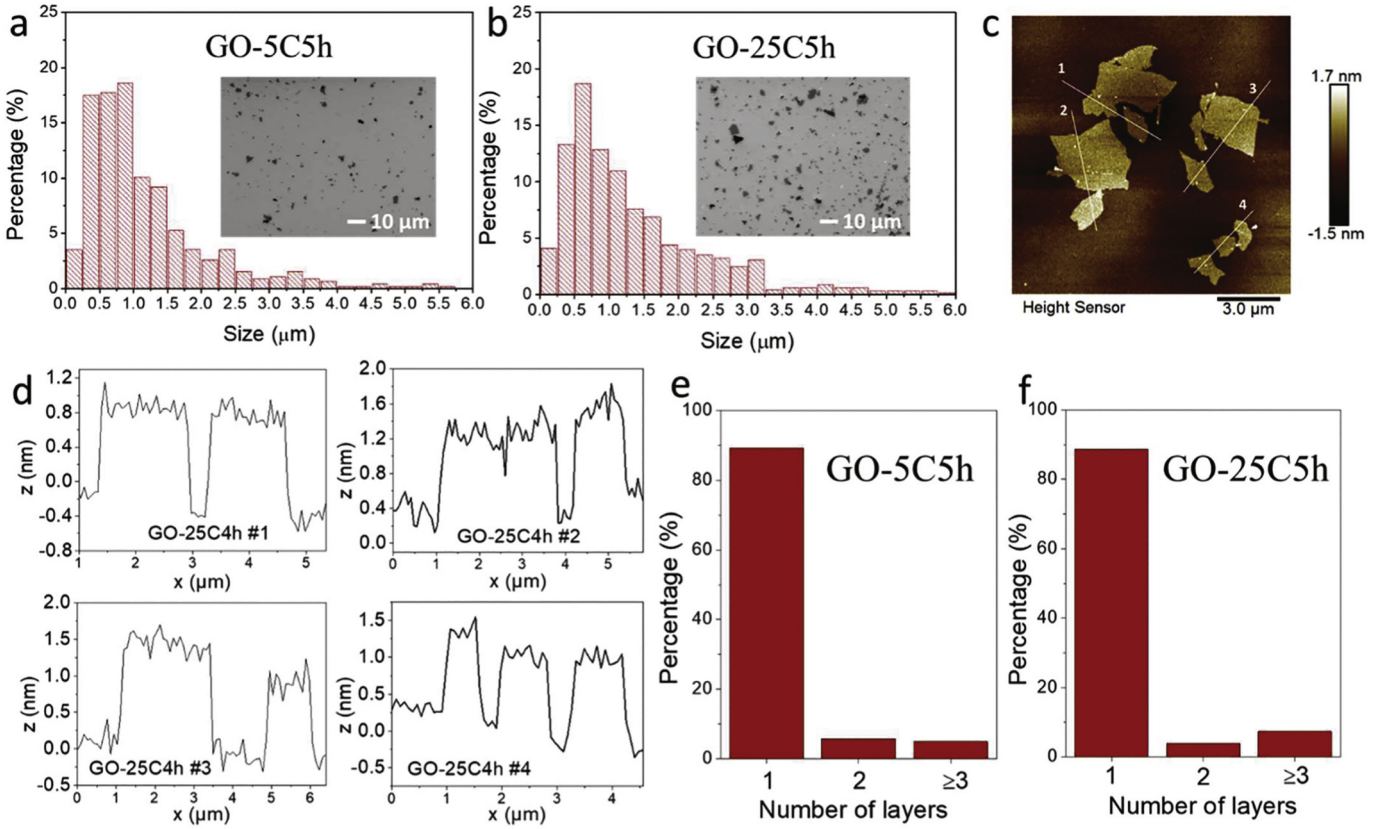

Fig. 2. Morphological characteristics of GO-5C5h and GO-25C5h. (a-b) Size distributions of GO sheets based on the SEM images (inset). (c) AFM image of GO-25C5h flakes and (d) the corresponding line profiles of the numbered flakes. (e-f) Distributions of number of layers based on 121 pieces of GO-5C5h sheets and 176 pieces of GO-25C5h sheets from AFM images.

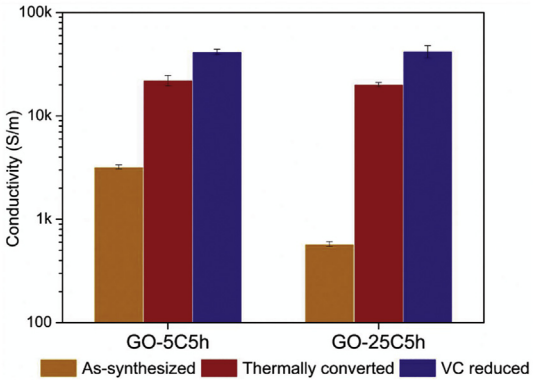

Fig. 3. Changes in the electrical conductivity of GO-5C5h and GO-25C5h before and after thermal conversion and chemical reduction.

structural integrity, in the course of thermal conversion and VC reduction. Raman spectra (Fig. 4a-b) exhibit the differences not only between thermal conversion and VC reduction, but also between the VC reduced GO-5C5h (VCrGO-5C5h) and GO-25C5h (VCrGO-25C5h). For the thermal conversion of both GO samples (Fig. 4a), neither D band nor G band underwent noticeable changes, as previously observed experimentally [57,59]. This is likely to be ascribed to the lattice damage induced by the thermal deoxygenation of GO [60], which offsets the restoration of sp^2 carbon. In contrast, in the case of VC reduction (Fig. 4b), the D and G bands notably sharpened, accompanied by a shrinkage in the inter-band regions between 1500 and 1550 cm^{-1} (also known as D" or D3 band) [61–63]. This indicates that the VCrGO samples were less disordered and amorphous than the original and thermally converted ones [44,48,64]. Meanwhile, a small shoulder appeared in the right side of G bands in VCrGO, tied to another defect-activated D' band centered at around 1620 cm^{-1} [46]. In addition to the narrower D and G bands, the greater I_D/I_G in the VCrGO samples, with respect to the unreduced or thermally converted states, suggests a decrease in the defect density and larger sp^2 carbon domains in the second stage when GO were subject to VC reduction [43,47]. Therefore, VC is more effective in reconstructing intact sp^2 domains in GO and thus restoring more conductivity than the thermal reduction.

To unveil the differences between the VCrGO-5C5h and VCrGO-25C5h, the Raman spectra GO and their precursors, namely GO-5C5h, GO-25C5h, VCrGO-5C5h and VCrGO-25C5h, are fitted into four components, including D, D", G and D' bands [64,65] (Fig. S11) and the fitting results have been summarized in Table S5. It can be observed that the I_D/I_G of the VCrGO-25C5h (2.05) is higher than that of the VCrGO-5C5h (1.77), while as aforementioned, the original GO-25C5h had a smaller I_D/I_G, or more defects, than the GO-5C5h. Based on the reduction in the I_D'/I_G ratio as well as the FWHM (full width at half maximum) of D, G and D' bands, the Raman fitting reveals that the GO-25C5h could regain more graphitic sp^2 domains together with reduced defects via VC reduction in comparison to the GO-5C5h [47,65]. This can also be confirmed by the sharper and stronger 2D band (~2700 cm^{-1}), which is the second order of D band [42], for the VCrGO-25C5h (Fig. 4b), as it is indicative of the more expanded sp^2 domains and less amorphous structure [66,67].

Aside from Raman spectroscopy, XPS was further employed to measure the changes in the oxygen functionalization of the VCrGO. The

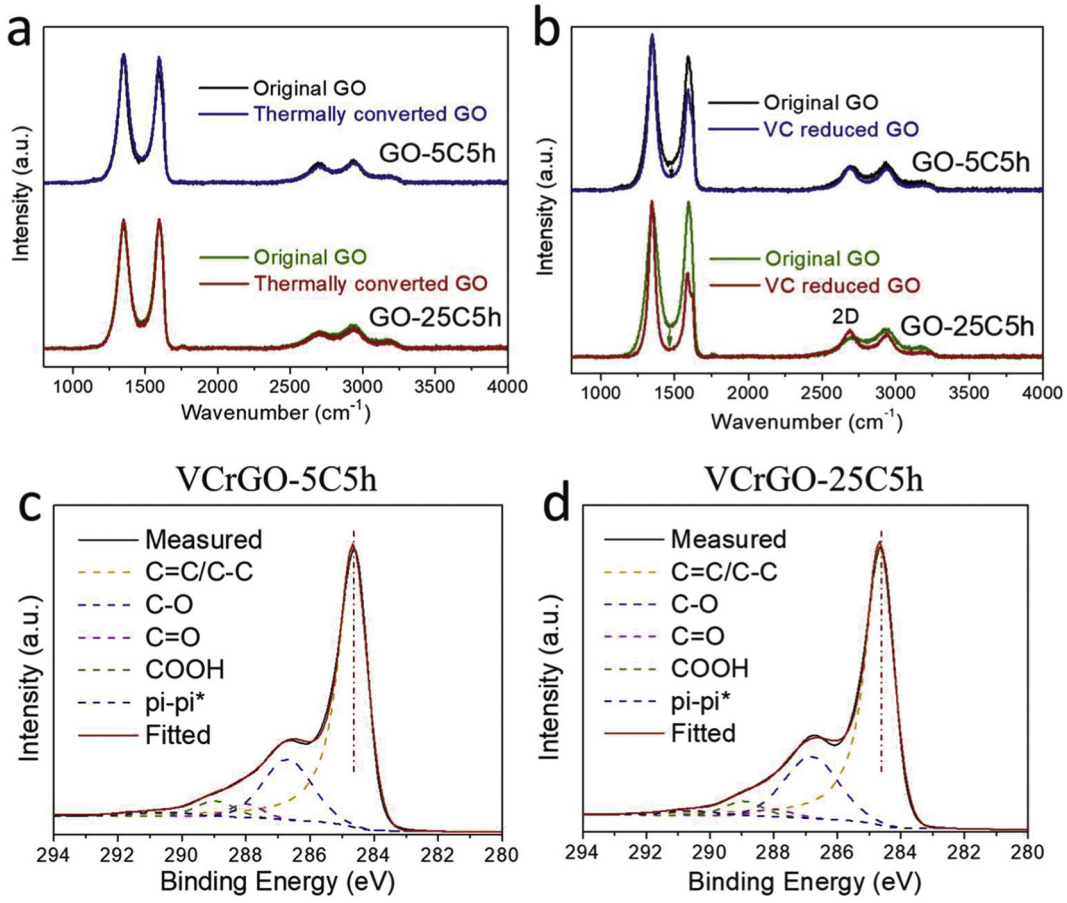

Fig. 4. Chemical characterizations of thermally converted and VC reduced GO. (a-b) Changes in the Raman spectra of GO-5C5h and GO-25C5h between original and reduced state. (c-d) XPS C 1 s spectra of the two VC reduced GO (VCrGO) samples. The dash-dotted lines indicate the asymmetrical shapes of the main peaks.

survey scan (Fig. S12) depicts that both VCrGO-5C5h and VCrGO-25C5h had the similar C/O ratio of around 4.9. Moreover, with respect to the unreduced state, the VCrGO-25C5h underwent a greater increase in C/O ratio from 3.40 to 4.88 than the VCrGO-5C5h (from 4.05 to 4.89), confirming that the GO-25C5h has more oxygen functional groups which were easily removed during VC reduction. In terms of XPS C 1 s spectra (Fig. 4c-d), the main peaks centered at around 284.6 eV are in the asymmetrical shape, probably attributed to the more conductive state of carbon in VCrGO [68]. Therefore, the C=C/C-C component in the VCrGO was fitted using a Doniach-Sunjic asymmetric line shape with zero asymmetry coefficient [69,70]. According to the C 1 s deconvolution results (Table S6), VCrGO-25C5h showed a larger growth in the fraction of graphitic carbon (C=C/C-C), from 54.62 at.% to 69.35 at.%, giving rise to the substantial enhancement in the conductivity of VCrGO-25C5h. This is consistent with the Raman data, which implied the more graphitic sp^2 domains restored during VC reduction. Additionally, the graphitic carbon content in the VCrGO-25C5h reached the same level of VCrGO-5C5h (70.24 at.%), which likely contributes to their similar electrical conductivity.

4. Conclusions

In this paper, we have further studied the chemical method to produce monolayered GO with excellent solution processability from expanded graphite at room temperature. The use of expanded graphite significantly facilitated the conversion to GO within only 5 h at both 5 °C and 25 °C. This allows a more rational comparison between low T-GO (at 5 °C) and RT-GO (at 25 °C) using the same synthesis conditions. We found that GO produced at 25 °C was able to recover considerably more electrical conductivity and eventually became as conductive as the counterpart prepared at 5 °C by either 150 °C thermal annealing or green VC reduction, despite the fact that the initial conductivity of the RT-GO was much lower than that of the low T-GO. In addition, VC reduction was found to be more effective in the enhancement of conductivity than the mild thermal treatment. Moreover, a wide range of characterization techniques revealed that the dramatic increase in the conductivity of RT-GO reduced by VC was attributed to the restoration of more intact graphitic sp^2 domains, and less amorphous and defective structure of rGO. Therefore, our work highlights the cost-effective, sustainable fabrication of high quality graphene materials with minimal energy input and environmentally-friendly reducing agents. For the future work, we will fulfill the potential of this RT-GO in more electroconductive applications, such as conductive binders for lithium ion batteries and wearable electronics.

Declaration of Competing Interest

The authors declare that they have no known competing financial interests or personal relationships that could have appeared to influence the work reported in this paper.

Acknowledgement

The authors acknowledge the support from the Australian Research Council (DP190100120, LP160101521 and FT160100207).

Appendix A. Supplementary data

Supplementary data to this article can be found online at https://doi.org/10.1016/j.susmat.2020.e00198.

References

[1] K.S. Novoselov, A.K. Geim, S.V. Morozov, D. Jiang, Y. Zhang, S.V. Dubonos, I.V. Grigorieva, A.A. Firsov, Electric field effect in atomically thin carbon films, Science 306 (5696) (2004) 666.
[2] A.K. Geim, K.S. Novoselov, The rise of graphene, Nat. Mater. 6 (3) (2007) 183–191.
[3] F. Bonaccorso, L. Colombo, G. Yu, M. Stoller, V. Tozzini, A.C. Ferrari, R.S. Ruoff, V. Pellegrini, Graphene, related two-dimensional crystals, and hybrid systems for energy conversion and storage, Science 347 (6217) (2015), 1246501.
[4] R. Raccichini, A. Varzi, S. Passerini, B. Scrosati, The role of graphene for electrochemical energy storage, Nat. Mater. 14 (2014) 271.
[5] Y. Yang, X. Yang, L. Liang, Y. Gao, H. Cheng, X. Li, M. Zou, R. Ma, Q. Yuan, X. Duan, Large-area graphene-nanomesh/carbon-nanotube hybrid membranes for ionic and molecular nanofiltration, Science 364 (6445) (2019) 1057–1062.
[6] L. Chen, G. Shi, J. Shen, B. Peng, B. Zhang, Y. Wang, F. Bian, J. Wang, D. Li, Z. Qian, G. Xu, G. Liu, J. Zeng, L. Zhang, Y. Yang, G. Zhou, M. Wu, W. Jin, J. Li, H. Fang, Ion sieving in graphene oxide membranes via cationic control of interlayer spacing, Nature 550 (2017) 380.
[7] K. Kostarelos, K.S. Novoselov, Graphene devices for life, Nat. Nanotechnol. 9 (2014) 744.
[8] C. Chung, Y.-K. Kim, D. Shin, S.-R. Ryoo, B.H. Hong, D.-H. Min, Biomedical applications of graphene and graphene oxide, Acc. Chem. Res. 46 (10) (2013) 2211–2224.
[9] D. Voiry, H.S. Shin, K.P. Loh, M. Chhowalla, Low-dimensional catalysts for hydrogen evolution and CO2 reduction, Nat. Rev. Chem. 2 (2018), 0105.
[10] G. Shi, S.E. Lowe, A.J.T. Teo, T.K. Dinh, S.H. Tan, J. Qin, Y. Zhang, Y.L. Zhong, H. Zhao, A versatile PDMS submicrobead/graphene oxide nanocomposite ink for the direct ink writing of wearable micron-scale tactile sensors, Appl. Mater. Today 16 (2019) 482–492.
[11] A. Zurutuza, C. Marinelli, Challenges and opportunities in graphene commercialization, Nat. Nanotechnol. 9 (2014) 730.
[12] Y.L. Zhong, Z. Tian, G.P. Simon, D. Li, Scalable production of graphene via wet chemistry: progress and challenges, Mater. Today 18 (2) (2015) 73–78.
[13] W.S. Hummers, R.E. Offeman, Preparation of graphitic oxide, J. Am. Chem. Soc. 80 (6) (1958)(1339–1339).
[14] A.M. Dimiev, J.M. Tour, Mechanism of Graphene oxide formation, ACS Nano 8 (3) (2014) 3060–3068.
[15] N.I. Kovtyukhova, P.J. Ollivier, B.R. Martin, T.E. Mallouk, S.A. Chizhik, E.V. Buzaneva, A.D. Gorchinskiy, Layer-by-layer assembly of ultrathin composite films from micron-sized graphite oxide sheets and polycations, Chem. Mater. 11 (3) (1999) 771–778.
[16] L. Dong, J. Yang, M. Chhowalla, K.P. Loh, Synthesis and reduction of large sized graphene oxide sheets, Chem. Soc. Rev. 46 (23) (2017) 7306–7316.
[17] Y. Xu, H. Bai, G. Lu, C. Li, G. Shi, Flexible Graphene films via the filtration of water-soluble noncovalent functionalized graphene sheets, J. Am. Chem. Soc. 130 (18) (2008) 5856–5857.
[18] D. Li, M.B. Müller, S. Gilje, R.B. Kaner, G.G. Wallace, Processable aqueous dispersions of graphene nanosheets, Nat. Nanotechnol. 3 (2008) 101.
[19] S.H. Aboutalebi, M.M. Gudarzi, Q.B. Zheng, J.-K. Kim, Spontaneous formation of liquid crystals in ultralarge graphene oxide dispersions, Adv. Funct. Mater. 21 (15) (2011) 2978–2988.
[20] L. Dong, Z. Chen, S. Lin, K. Wang, C. Ma, H. Lu, Reactivity-controlled preparation of ultralarge graphene oxide by chemical expansion of graphite, Chem. Mater. 29 (2) (2017) 564–572.
[21] D.C. Marcano, D.V. Kosynkin, J.M. Berlin, A. Sinitskii, Z. Sun, A. Slesarev, L.B. Alemany, W. Lu, J.M. Tour, Improved synthesis of graphene oxide, ACS Nano 4 (8) (2010) 4806–4814.
[22] J. Chen, B. Yao, C. Li, G. Shi, An improved Hummers method for eco-friendly synthesis of graphene oxide, Carbon 64 (2013) 225–229.
[23] W. Ren, H.-M. Cheng, The global growth of graphene, Nat. Nanotechnol. 9 (2014) 726.
[24] X.-Y. Wang, A. Narita, K. Müllen, Precision synthesis versus bulk-scale fabrication of graphenes, Nat. Rev. Chem. 2 (2017), 0100.
[25] S. Eigler, M. Enzelberger-Heim, S. Grimm, P. Hofmann, W. Kroener, A. Geworski, C. Dotzer, M. Röckert, J. Xiao, C. Papp, O. Lytken, H.-P. Steinrück, P. Müller, A. Hirsch, Wet chemical synthesis of graphene, Adv. Mater. 25 (26) (2013) 3583–3587.
[26] B. Butz, C. Dolle, C.E. Halbig, E. Spiecker, S. Eigler, Highly intact and pure oxo-functionalized graphene: synthesis and electron-beam-induced reduction, Angew. Chem. Int. Ed. 55 (51) (2016) 15771–15774.
[27] D. Voiry, J. Yang, J. Kupferberg, R. Fullon, C. Lee, H.Y. Jeong, H.S. Shin, M. Chhowalla, High-quality graphene via microwave reduction of solution-exfoliated graphene oxide, Science 353 (6306) (2016) 1413–1416.
[28] J. Qin, Y. Zhang, S.E. Lowe, L. Jiang, H.Y. Ling, G. Shi, P. Liu, S. Zhang, Y.L. Zhong, H. Zhao, Room temperature production of graphene oxide with thermally labile oxygen functional groups for improved lithium ion battery fabrication and performance, J. Mater. Chem. A 7 (16) (2019) 9646–9655.
[29] H. Chen, W. Du, J. Liu, L. Qu, C. Li, Efficient room-temperature production of high-quality graphene by introducing removable oxygen functional groups to the precursor, Chem. Sci. 10 (4) (2019) 1244–1253.
[30] M. Zhang, Y. Wang, L. Huang, Z. Xu, C. Li, G. Shi, Multifunctional pristine chemically modified graphene films as strong as stainless steel, Adv. Mater. 27 (42) (2015) 6708–6713.
[31] Z. Luo, Y. Lu, L.A. Somers, A.T.C. Johnson, High yield preparation of macroscopic graphene oxide membranes, J. Am. Chem. Soc. 131 (3) (2009) 898–899.
[32] L. Sun, B. Fugetsu, Mass production of graphene oxide from expanded graphite, Mater. Lett. 109 (2013) 207–210.
[33] X. Li, G. Zhang, X. Bai, X. Sun, X. Wang, E. Wang, H. Dai, Highly conducting graphene sheets and Langmuir–Blodgett films, Nat. Nanotechnol. 3 (9) (2008) 538–542.
[34] D. Cai, M. Song, Preparation of fully exfoliated graphite oxide nanoplatelets in organic solvents, J. Mater. Chem. 17 (35) (2007) 3678–3680.
[35] S.E. Lowe, G. Shi, Y. Zhang, J. Qin, S. Wang, A. Uijtendaal, J. Sun, L. Jiang, S. Jiang, D. Qi, M. Al-Mamun, P. Liu, Y.L. Zhong, H. Zhao, Scalable production of graphene oxide

using a 3D-printed packed-bed electrochemical reactor with a boron-doped diamond electrode, ACS Appl. Nano Mater. 2 (2) (2019) 867–878.
[36] S. Park, J. An, J.R. Potts, A. Velamakanni, S. Murali, R.S. Ruoff, Hydrazine-reduction of graphite- and graphene oxide, Carbon 49 (9) (2011) 3019–3023.
[37] P. Yu, Z. Tian, S.E. Lowe, J. Song, Z. Ma, X. Wang, Z.J. Han, Q. Bao, G.P. Simon, D. Li, Y. Zhong, Mechanically-assisted electrochemical production of graphene oxide, Chem. Mater. 28 (22) (2016) 8429–8438.
[38] Z.-J. Fan, W. Kai, J. Yan, T. Wei, L.-J. Zhi, J. Feng, Y.-m. Ren, L.-P. Song, F. Wei, Facile synthesis of graphene nanosheets via Fe reduction of exfoliated graphite oxide, ACS Nano 5 (1) (2011) 191–198.
[39] K. Fu, Y. Wang, C. Yan, Y. Yao, Y. Chen, J. Dai, S. Lacey, Y. Wang, J. Wan, T. Li, Z. Wang, Y. Xu, L. Hu, Graphene oxide-based electrode inks for 3D-printed lithium-ion batteries, Adv. Mater. 28 (13) (2016) 2587–2594.
[40] Z. Xu, Y. Zhang, P. Li, C. Gao, Strong, conductive, lightweight, neat graphene aerogel fibers with aligned pores, ACS Nano 6 (8) (2012) 7103–7113.
[41] W. Gao, L.B. Alemany, L. Ci, P.M. Ajayan, New insights into the structure and reduction of graphite oxide, Nat. Chem. 1 (5) (2009) 403–408.
[42] A.C. Ferrari, J.C. Meyer, V. Scardaci, C. Casiraghi, M. Lazzeri, F. Mauri, S. Piscanec, D. Jiang, K.S. Novoselov, S. Roth, A.K. Geim, Raman spectrum of graphene and graphene layers, Phys. Rev. Lett. 97 (18) (2006), 187401.
[43] A.C. Ferrari, S.E. Rodil, J. Robertson, Interpretation of infrared and Raman spectra of amorphous carbon nitrides, Phys. Rev. B Condens. Matter 67 (15) (2003), 155306.
[44] E.H. Martins Ferreira, M.V.O. Moutinho, F. Stavale, M.M. Lucchese, R.B. Capaz, C.A. Achete, A. Jorio, Evolution of the Raman spectra from single-, few-, and many-layer graphene with increasing disorder, Phys. Rev. B Condens. Matter 82 (12) (2010) 125429.
[45] L.G. Cançado, A. Jorio, E.H.M. Ferreira, F. Stavale, C.A. Achete, R.B. Capaz, M.V.O. Moutinho, A. Lombardo, T.S. Kulmala, A.C. Ferrari, Quantifying defects in graphene via Raman spectroscopy at different excitation energies, Nano Lett. 11 (8) (2011) 3190–3196.
[46] A.C. Ferrari, D.M. Basko, Raman spectroscopy as a versatile tool for studying the properties of graphene, Nat. Nanotechnol. 8 (2013) 235.
[47] S. Eigler, C. Dotzer, A. Hirsch, Visualization of defect densities in reduced graphene oxide, Carbon 50 (10) (2012) 3666–3673.
[48] A.C. Ferrari, J. Robertson, Interpretation of Raman spectra of disordered and amorphous carbon, Phys. Rev. B Condens. Matter 61 (20) (2000) 14095–14107.
[49] S. Park, R.S. Ruoff, Chemical methods for the production of graphenes, Nat. Nanotechnol. 4 (4) (2009) 217–224.
[50] J. Chen, K. Sheng, P. Luo, C. Li, G. Shi, Graphene hydrogels deposited in nickel foams for high-rate electrochemical capacitors, Adv. Mater. 24 (33) (2012) 4569–4573.
[51] H. Feng, R. Cheng, X. Zhao, X. Duan, J. Li, A low-temperature method to produce highly reduced graphene oxide, Nat. Commun. 4 (1) (2013), 1539.
[52] H.A. Becerril, J. Mao, Z. Liu, R.M. Stoltenberg, Z. Bao, Y. Chen, Evaluation of solution-processed reduced graphene oxide films as transparent conductors, ACS Nano 2 (3) (2008) 463–470.
[53] K.K.H. De Silva, H.H. Huang, R.K. Joshi, M. Yoshimura, Chemical reduction of graphene oxide using green reductants, Carbon 119 (2017) 190–199.
[54] Z. Xie, H.L. Tan, X. Wen, Y. Suzuki, A. Iwase, A. Kudo, R. Amal, J. Scott, Y.H. Ng, The importance of the interfacial contact: is reduced graphene oxide always an enhancer in photo(electro)catalytic water oxidation? ACS Appl. Mater. Interfaces 11 (26) (2019) 23125–23134.
[55] H.L. Tan, H.A. Tahini, X. Wen, R.J. Wong, X. Tan, A. Iwase, A. Kudo, R. Amal, S.C. Smith, Y.H. Ng, Interfacing BiVO4 with reduced graphene oxide for enhanced Photoactivity: a tale of facet dependence of electron shuttling, Small 12 (38) (2016) 5295–5302.
[56] J. Zhang, H. Yang, G. Shen, P. Cheng, J. Zhang, S. Guo, Reduction of graphene oxide vial-ascorbic acid, Chem. Commun. 46 (7) (2010) 1112–1114.
[57] S. Eigler, S. Grimm, M. Enzelberger-Heim, P. Müller, A. Hirsch, Graphene oxide: efficiency of reducing agents, Chem. Commun. 49 (67) (2013) 7391–7393.
[58] K.K.H. De Silva, H.-H. Huang, M. Yoshimura, Progress of reduction of graphene oxide by ascorbic acid, Appl. Surf. Sci. 447 (2018) 338–346.
[59] D. Zhan, Z. Ni, W. Chen, L. Sun, Z. Luo, L. Lai, T. Yu, A.T.S. Wee, Z. Shen, Electronic structure of graphite oxide and thermally reduced graphite oxide, Carbon 49 (4) (2011) 1362–1366.
[60] R. Larciprete, S. Fabris, T. Sun, P. Lacovig, A. Baraldi, S. Lizzit, Dual path mechanism in the thermal reduction of Graphene oxide, J. Am. Chem. Soc. 133 (43) (2011) 17315–17321.
[61] G.A. Zickler, B. Smarsly, N. Gierlinger, H. Peterlik, O. Paris, A reconsideration of the relationship between the crystallite size La of carbons determined by X-ray diffraction and Raman spectroscopy, Carbon 44 (15) (2006) 3239–3246.
[62] A. Sadezky, H. Muckenhuber, H. Grothe, R. Niessner, U. Pöschl, Raman microspectroscopy of soot and related carbonaceous materials: spectral analysis and structural information, Carbon 43 (8) (2005) 1731–1742.
[63] J.D. Herdman, B.C. Connelly, M.D. Smooke, M.B. Long, J.H. Miller, A comparison of Raman signatures and laser-induced incandescence with direct numerical simulation of soot growth in non-premixed ethylene/air flames, Carbon 49 (15) (2011) 5298–5311.
[64] S. Claramunt, A. Varea, D. López-Díaz, M.M. Velázquez, A. Cornet, A. Cirera, The importance of interbands on the interpretation of the Raman spectrum of GRAPHENE oxide, J. Phys. Chem. C 119 (18) (2015) 10123–10129.
[65] A. Eckmann, A. Felten, A. Mishchenko, L. Britnell, R. Krupke, K.S. Novoselov, C. Casiraghi, Probing the nature of defects in graphene by Raman spectroscopy, Nano Lett. 12 (8) (2012) 3925–3930.
[66] A. Ganguly, S. Sharma, P. Papakonstantinou, J. Hamilton, Probing the thermal deoxygenation of graphene oxide using high-resolution in situ X-ray-based spectroscopies, J. Phys. Chem. C 115 (34) (2011) 17009–17019.
[67] M.S. Dresselhaus, A. Jorio, M. Hofmann, G. Dresselhaus, R. Saito, Perspectives on carbon nanotubes and graphene Raman spectroscopy, Nano Lett. 10 (3) (2010) 751–758.
[68] A. Ouerghi, A. Kahouli, D. Lucot, M. Portail, L. Travers, J. Gierak, J. Penuelas, P. Jegou, A. Shukla, T. Chassagne, M. Zielinski, Epitaxial graphene on cubic SiC(111)/Si(111) substrate, Appl. Phys. Lett. 96 (19) (2010), 191910.
[69] C. Mattevi, G. Eda, S. Agnoli, S. Miller, K.A. Mkhoyan, O. Celik, D. Mastrogiovanni, G. Granozzi, E. Garfunkel, M. Chhowalla, Evolution of electrical, chemical, and structural properties of transparent and conducting chemically derived graphene thin films, Adv. Funct. Mater. 19 (16) (2009) 2577–2583.
[70] S. Kim, S. Zhou, Y. Hu, M. Acik, Y.J. Chabal, C. Berger, W. de Heer, A. Bongiorno, E. Riedo, Room-temperature metastability of multilayer graphene oxide films, Nat. Mater. 11 (6) (2012) 544–549.